ADVANCED FUNCTIONAL MATERIALS
www.afm-journal.de

Efficient Synthesis of Heteroatom (N or S)-Doped Graphene Based on Ultrathin Graphene Oxide-Porous Silica Sheets for Oxygen Reduction Reactions

Shubin Yang, Linjie Zhi, Kun Tang, Xinliang Feng,* Joachim Maier, and Klaus Müllen**

Heteroatom (N or S)-doped graphene with high surface area is successfully synthesized via thermal reaction between graphene oxide and guest gases (NH_3 or H_2S) on the basis of ultrathin graphene oxide-porous silica sheets at high temperatures. It is found that both N and S-doping can occur at annealing temperatures from 500 to 1000 °C to form the different binding configurations at the edges or on the planes of the graphene, such as pyridinic-N, pyrrolic-N, and graphitic-N for N-doped graphene, thiophene-like S, and oxidized S for S-doped graphene. Moreover, the resulting N and S-doped graphene sheets exhibit good electrocatalytic activity, long durability, and high selectivity when they are employed as metal-free catalysts for oxygen reduction reactions. This approach may provide an efficient platform for the synthesis of a series of heteroatom-doped graphenes for different applications.

1. Introduction

Graphene, a two-dimensional aromatic monolayer of carbon atoms, has attracted great attention owing to its exceptional physical,[1] chemical[2] and mechanical[3] properties as well as its potential applications in electronics,[4] sensors,[5] supercapacitors[6] and batteries.[7–10] Both theoretical and experimental studies[11–13] have revealed that chemical doping of graphene with foreign atoms such as nitrogen, boron and sulfur can tailor its electronic property and chemical reactivity, as well as give rise to new functions. A particularly exciting example is N-doped graphene (NG) that exhibits high electrocatalytic activity and CO tolerance in comparison to conventional platinum catalysts for oxygen reduction reaction (ORR), and thus holds great promise to replace noble metal catalysts in fuel cells.[14,15] Up to now, several approaches such as chemical vapor deposition (CVD),[16] arc-discharge,[17] and thermal annealing of graphene oxide under ammonia atmosphere,[18] have been developed to produce B and/or N-doped graphene sheets. However, high vacuum conditions during the above synthesis are usually inevitable and the resulting B and N-doped graphene commonly contain multilayers in addition to the single layers.[16,17] Further, the synthesis of other heteroatom-doped graphenes for example by incorporation of sulfur remains a big challenge. Given that single-layer graphene oxide can be readily available in large quantities by the Hummers method,[19] thermal reaction of graphene oxide with guest gases such as ammonia at relatively high temperatures should provide a feasible protocol towards the large-scale production of heteroatom-doped graphene.[18] Although this is easy to imagine, the actual operation is difficult because the direct thermal annealing process generally results in an irreversible stacking of graphene due to the strong π-interactions.[20,21] As a consequence, the specific surface area of the resulting graphene materials is low (<500 m^2 g^{-1}), which hampers their physical and chemical properties.[20,21]

In this article, we describe an efficient synthesis of heteroatom (N or S)-doped graphene via a thermal reaction between graphene oxide and guest gases (NH_3 or H_2S) based on our graphene oxide-mesoporous silica (GO-silica) sheets. Thereby, each graphene oxide sheet is fully confined within a thin and porous silica shell.[9] By this means, the unique porous silica layer: 1) can favor the transport of the gas source to the surface of graphene oxide that facilitates the thermal reaction and 2) can effectively prevent the irreversible re-aggregation of graphene during the heteroatom doping process at high temperature. As a result, nitrogen and sulfur-doped graphenes with high surface areas can be achieved. Moreover, we demonstrate that the resulting N and S-doped graphenes can serve as metal-free electrocatalysts for the oxygen reduction reactions, showing comparable electrocatalytic activity to that of commercially available Pt/C.

Dr. S. B. Yang, Prof. X. L. Feng, Prof. K. Müllen
Max Planck Institute for Polymer Research
Ackermannweg 10, 55128, Germany
E-mail: feng@mpip-mainz.mpg.de;
muellen@mpip-mainz.mpg.de
Prof. L. J. Zhi
National Center for Nanoscience and Technology of China
Beiyitiao 11, 100190, China
Dr. K. Tang, Prof. J. Maier
Max Planck Institute for Solid State Research
Heisenberg Str. 1, 70569, Germany
E-mail: k.tang@fkf.mpg.de
Prof. X. L. Feng
School of Chemistry and Chemical Engineering
Shanghai Jiao Tong University
800 Dongchuan Road, Shanghai 200240, China

DOI: 10.1002/adfm.201200186

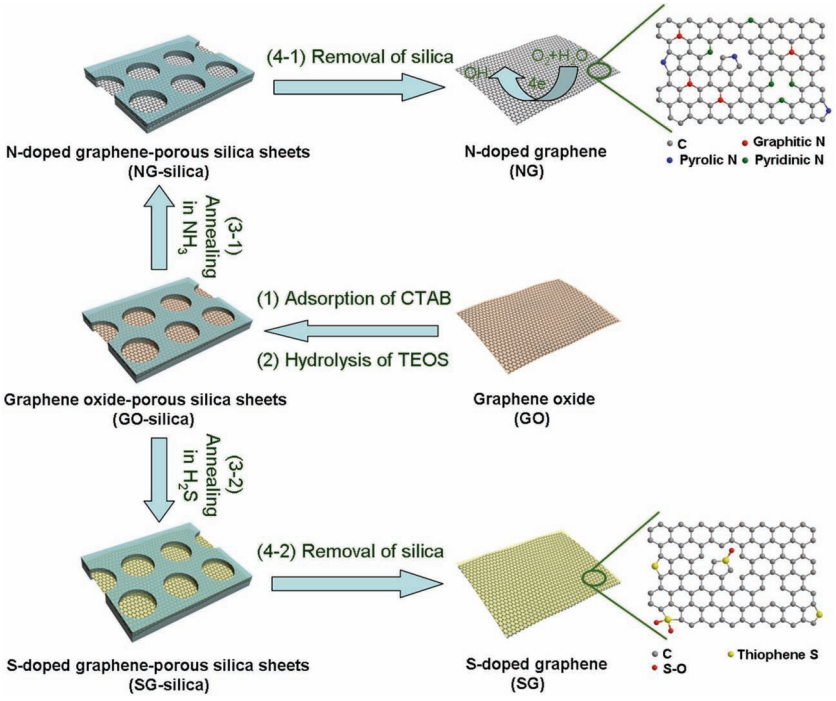

Scheme 1. Schematic illustration of the fabrication of N and S-doped graphene: (1) and (2) hydrolysis of TEOS around the surface of graphene oxide with the aid of a cationic surfactant, cetyltrimethyl ammonium bromide (CTAB); (3-1) thermal annealing of GO-Silica sheets in ammonia at 600, 800, 900 and 1000 °C, respectively; (3-2) thermal annealing of GO-Silica sheets in H_2S gas at 500, 700 and 900 °C, respectively; and (4-1 and 4-2) removal of silica by HF or NaOH solution.

2. Results and Discussion

2.1. Preparation and Characterization of Heteroatom-Doped Graphene

As illustrated in **Scheme 1**, the thin, sandwich-like graphene oxide-porous silica (GO-silica) sheets were first fabricated via the hydrolysis of tetraethyl orthosilicate (TEOS) on the surface of graphene oxide with the aid of a cationic surfactant, cetyltrimethyl ammonium bromide (CTAB).[9] Subsequently, the resulting porous nanosheets were subjected to annealing under NH_3 or H_2S atmosphere at different temperatures (500–1000 °C), where the abundant functional groups such as carbonyl, carboxyl, lactone and quinone at the edges and in the plane of graphene oxide were favorable for the binding of nitrogen[18] and sulfur. After removal of silica by etching with 10% HF or 2M NaOH solution, fully isolated N and S-doped graphene sheets were generated, which are denoted as NGX and SGX, respectively, where X represents the annealing temperature.

The morphology and structure of as-prepared graphene oxide-porous silica sheets were first investigated via transmission electron microscopy (TEM) with energy-dispersive X-ray (EDX) analysis and atomic force microscopy (AFM). As shown in **Figure 1**a, many nanosheets with similar morphology to that of graphene oxide can be distinctly observed. Remarkably enough, these sheets possess numerous mesopores with the size of about 2 nm and a high Brunauer–Emmett–Teller (BET) surface area of 1051 $m^2\ g^{-1}$ (Figure 1b,d and Supporting Information Figure S1). EDX and elemental mapping further reveals that graphene oxide is confined in silica layers as expected (Supporting Information Figure S2). Moreover, the resulting GO-silica sheets are highly transparent to electron beams as displayed in the TEM image (Figure 1a) which are even comparable to that of the graphene oxide sheets, indicating their ultrathin nature. Cross-sectional AFM analyses were further conducted to investigate the structural features of GO-silica sheets. Typical AFM images support the morphological conclusions drawn form from TEM observations and a thickness analysis reveals a uniform thickness of about 15 nm (Figure 1c). Notably, the resulting sheets are much thinner than those in our previously reported GO-silica sheets (about 30 nm). Thus, one can expect that these thin sheets

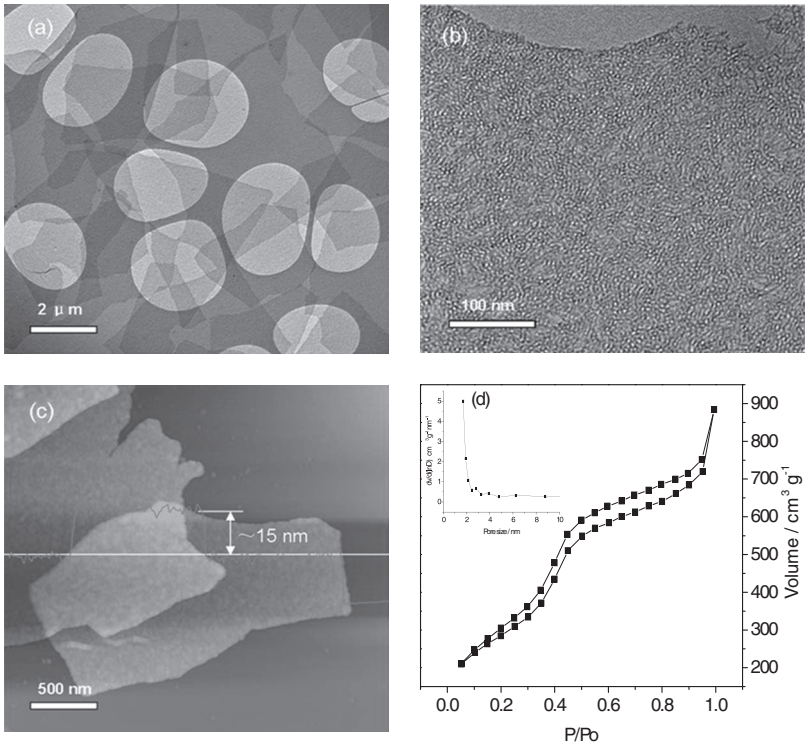

Figure 1. a,b) Typical TEM and c) AFM images of GO-porous silica sheets with different magnifications. d) Nitrogen adsorption/desorption isotherm of GO-porous silica sheets (inset: pore size distribution), demonstrating the porous structure with the pore size of about 2 nm and a high BET surface area of 1051 $m^2\ g^{-1}$.

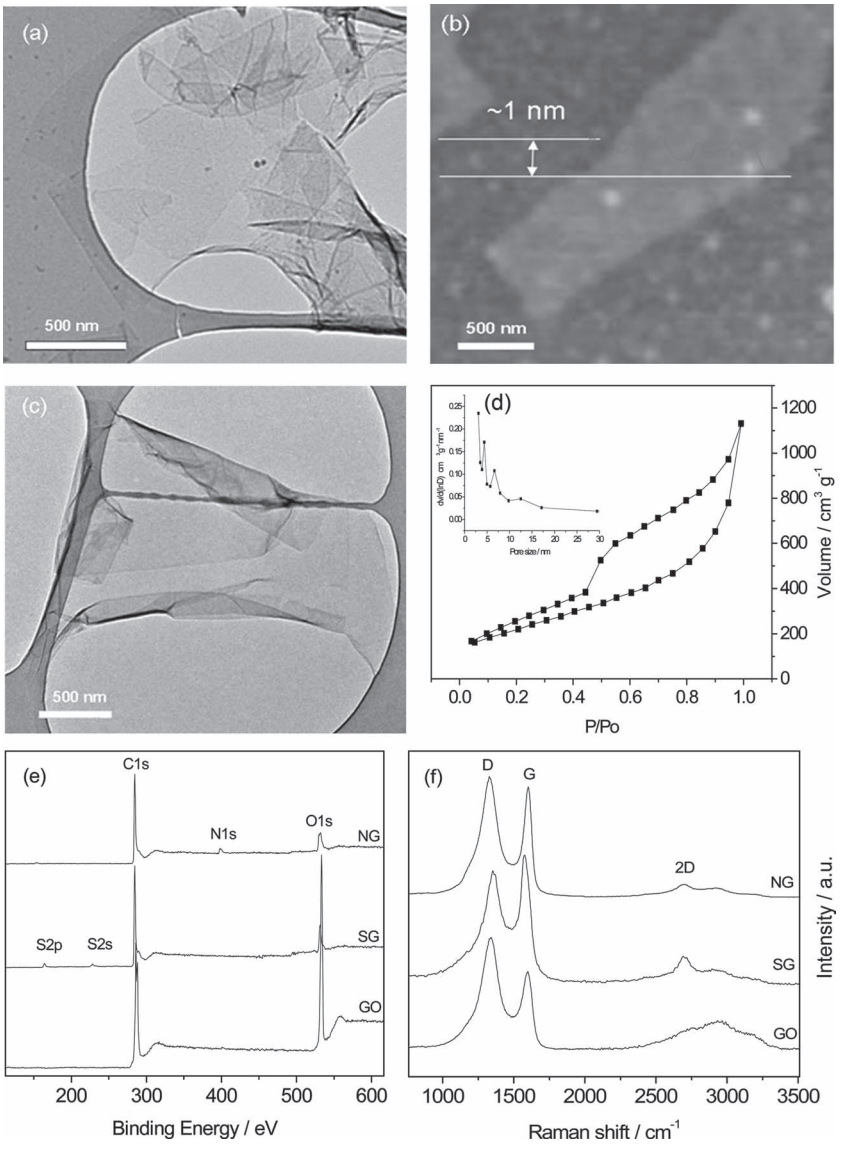

Figure 2. a) Typical TEM and b) AFM images of NG. c) Typical TEM image of SG. d) Nitrogen adsorption/desorption isotherm of N-doped graphene (inset: pore size distribution), revealing that the BET surface area of NG is 816 $m^2 g^{-1}$. e) XPS survey spectra and f) Raman spectra of GO, SG, and NG, respectively.

will be particularly favorable in allowing for the access of NH_3 and H_2S gas to the surface of graphene oxide for the simultaneous heteroatom doping and reduction of GO.

As demonstrated in **Figure 2**, N and S-doped graphene sheets with a laminar morphology like silk veil waves are obtained after thermal annealing of GO-silica sheets in NH_3 and H_2S gas at high temperatures and subsequent removal of silica. The morphology is similar to that reported for reduced graphene oxide[22] and the partially crinkled nature may originate from the defective structures formed during the fabrication of GO and the heteroatom doping processes. The AFM analysis (Figure 2b) further discloses the same morphology as observed by TEM (Figure 2a,c) with a thickness of about 1 nm, confirming the single-layer feature. The typical nitrogen adsorption and desorption curve of the resulting heteroatom-doped graphene displays a high BET surface area of 816 $m^2 g^{-1}$ (Figure 2d). Although this value is still lower than the theoretical value of 2630 $m^2 g^{-1}$ for single-layer graphene,[23] it is much higher than those reported for graphene and N-doped graphene (typically in the range of 200 to 500 $m^2 g^{-1}$).[24,25] Moreover, the single-layer nature of heteroatom-doped graphene with ultrahigh surface area can be well maintained by simple transformation into other sandwich-like, graphene-based materials via a conversional nanocasting process, in which heteroatom-doped graphene-porous silica is employed as a template.[9]

X-ray photoelectron spectroscopy (XPS) and Raman spectroscopy measurements were conducted to elucidate the chemical structure of the resulting SG and NG sheets. Apparently, nitrogen and sulfur signals can be observed in the XPS spectra of NG and SG (Figure 2e), respectively, suggesting that both N and S species have been successfully incorporated into graphene. In addition to the heteroatom doping, high temperature annealing of GO-silica sheets in the presence of NH_3 and H_2S also has an influence on the reduction degree on graphene oxide. As presented in **Figure 3**a,d, the peak at a high binding energy of 286.5 eV in C1s XPS spectrum of GO sheets is nearly eliminated upon thermal treatment above 500 °C. This suggests that the large amounts of oxygen-functional groups such as C-O bonds, carbonyls (C = O), and carboxylates (O-C = O) on[18] GO are largely removed (see Supporting Information Figure S3). On the basis of elemental analysis, a significant decrease of the oxygen content from about 35% for GO to 5% for NG and SG is observed. Raman analysis further confirmed the reduction process of GO (Figure 2f and Supporting Information Figure S4). The typical Raman spectra of NG and SG exhibit two remarkable peaks at about 1330 and 1600 cm^{-1}, corresponding to the D and G band, respectively.[26] Clearly, the intensities of the D band of NG and SG become lower than that of GO (I_D/I_G = 1.46, see Supporting Information Figure S4), indicating that the graphitic degree of NG and SG is improved. Furthermore, with the increase of the annealing temperature, the I_D/I_G values of both NG and SG decrease, corresponding to the higher graphitic degree of NG and SG. In addition, comparing the I_D/I_G value of NG and SG annealed at the same temperature, we find that the I_D/I_G value of SG is lower than that of NG. This may be ascribed to the lower level of S-doping than N-doping on graphene (see below).

To probe the chemical state of nitrogen and sulphur in the heteroatom-doped graphene sheets, we analyzed the high

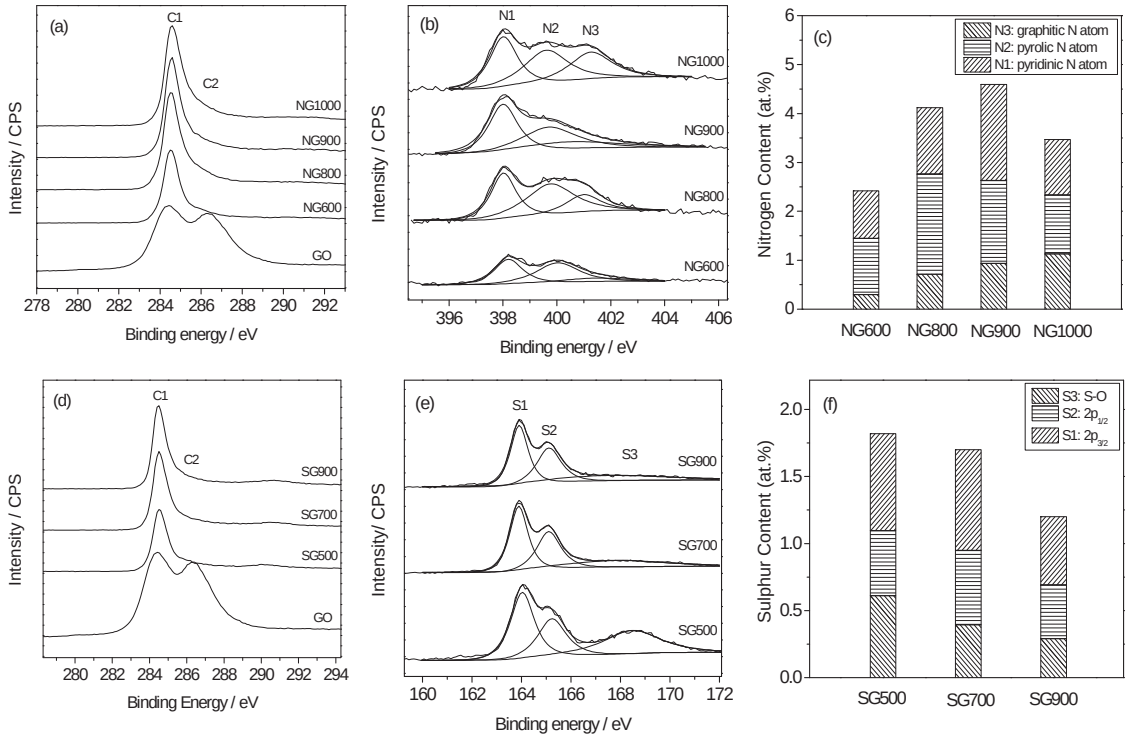

Figure 3. a) High resolution C1s XPS spectra of GO and NG with C1 (sp2 carbon in graphene) and C2 (sp3 carbon with C-O bonds, carbonyls (C=O), and carboxylates (O-C = O), originating from harsh oxidation). b) High resolution N1s XPS spectra of NG. The peaks are fitted to three energy components centered at around 398.0, 400.0, and 401.3 eV, corresponding to pyridinic-N (N1), pyrrolic-N (N2), and graphitic-N (N3), respectively. c) The content of three nitrogen species (N1, N2, and N3) in NG sheets. d) High resolution C1s XPS spectra of GO and SG with C1 and C2. e) High resolution S2p XPS spectra of SG. The peaks are fitted to three energy components centered at around 163.9, 165.1 and 168.5 eV, corresponding to $Sp_{3/2}$ (S1), $Sp_{1/2}$ (S2), and S-O (S3), respectively. f) The content of sulfur species (S1, S2, and S3) in SG sheets.

resolution N1s peaks of NG and S2p peaks of SG. As shown in Figure 3, all the NG samples exhibit an obvious N1s signal and the N content of NG is in the range of 2.4–4.6%, with the highest content for NG900. The complex N1s spectra can be further deconvoluted into three different peaks at the binding energies of ~398.0, 400.0 and 401.3 eV, corresponding to pyridinic-N (N1), pyrrolic-N (N2) and graphitic-N (N3) respectively.[15,27,28] Remarkably, the shape of these three peaks significantly changes with increasing the annealing temperature, indicating that different amounts of N bonding configurations are formed during the reaction of GO-silica sheets and NH_3 at various temperatures. It is worthy to note that, with the increase of temperature from 600 to 1000 °C, the highest energy peak N3 becomes dominant, implying that more graphitic N atoms are incorporated into the carbon network of graphene (Figure 3b). Differently, when the annealing temperature is increased from 900 to 1000 °C, the contents of pyridinic and pyrolic N largely decrease (Figure 3c) possibly owing to their lower stability at high temperature. Such a phenomenon is consistent with observation made for thermally pyrolyzed N-containing carbon materials.[27,29]

In comparison, all the high resolution S2p peaks of SG prepared at different temperatures can be again resolved into three different peaks at the binding energies of ~163.9, 165.1 and 168.5 eV, respectively (Figure 3e). The former two peaks are in agreement with the reported $2p_{3/2}$ (S1) and $2p_{1/2}$ (S2) positions of thiophene-S owing to their spin-orbit coupling.[30,31] The third peak should arise from some oxidized sulfur (S3)[31,32] in SG, whose XPS intensity significantly decreases with increasing the annealing temperature, indicating the lower stability of such species at higher temperature. Other sulfur components such as thiol (SH) at around 162.0 eV[30,33] can not be detected in the XPS spectra. Thereby, it can be inferred that the sulfur is mainly doped at the edges and defects of graphene in the form of thiophene-like structures at higher temperature (>700 °C). This stands in contrast to nitrogen doped graphene in which several N binding configurations in the hexagonal network of graphene can exist, like pyridinic- and graphitic-N. As a result, the overall content of sulfur in the SG prepared at 500–900 °C is only in the range of 1.2–1.7%, much lower than the nitrogen content (2.4–4.6%) in NG. To the best of our knowledge, this is the first detection of sulfur doping of graphene.

2.2. Electrocatalytic Properties of Heteroatom-Doped Graphene

One of the promising applications of the resulting heteroatom-doped graphenes can be envisaged in fuel cells as electrocatalyst for ORR.[34,35] It constitutes an ideal model material free of any metal for understanding whether nitrogen or sulfur incorporated into the graphene structure is electrocatalytically active in

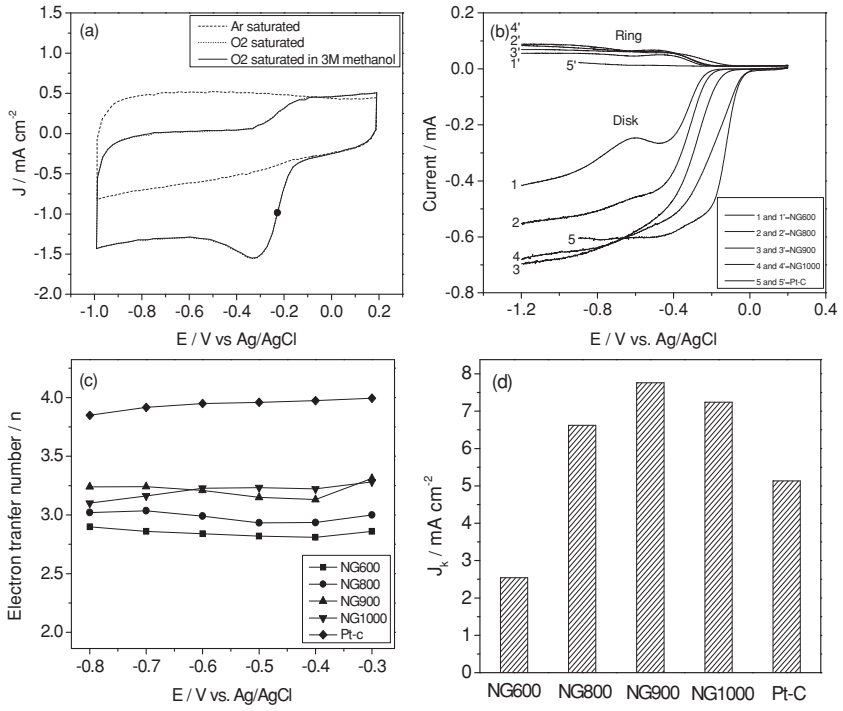

Figure 4. Electrocatalytic activity of N-doped graphene for ORR. a) Typical cyclic voltammograms of NG at a scan rate of 100 mV s^{-1} in O_2 and Ar-saturated 0.1 M KOH solution as well as O_2-saturated 0.1 M KOH solution with 3M methanol. b) Rotating ring disk electrode (RRDE) linear sweep voltammograms of NG600, NG800, NG 900, NG1000, and Pt-C at a rotation rate of 1600 rpm. c) The dependence of electron transfer number (n) on potential for NG600, NG800, NG 900, NG1000, and Pt-C. d) Electrochemical activity given as the kinetic-limiting current density (J_k) at –0.50 V for all NG and Pt-C.

the oxygen reduction. The electrocatalytic activity of the resulting N-doped graphene towards ORR was initially investigated with respect to commercial Pt-C (30 wt% platinum on carbon black) via cyclic voltammetry (CV) in 0.1 M KOH solution saturated with argon or oxygen. As shown in **Figure 4**a, a quasi-rectangular voltammogram without any evident peak in the potential range from –1.0 to +0.2 V, typical of high-surface-area carbons and supercapacitor performance,[36] is observed for NG in the argon-saturated solution. In contrast, a well-defined cathodic peak centered at –0.32 V appears in the CV when the electrolyte solution is saturated with O_2, similar to that of commercial Pt-C (Supporting Information Figure S5), suggesting a pronounced electrocatalytic activity of the as-prepared NG for oxygen reduction.

To gain further insight into the kinetics of the oxygen reduction reaction on NG, rotating ring disk electrode (RRDE) linear sweep voltammetry was performed in O_2-saturated 0.1 M KOH solution at a scanning rate of 10 mV s^{-1}. As shown in Figure 4b, the onset potential of NG increases positively from –0.23 to –0.04 V, close to that of commercial Pt-C (–0.04 V) as the annealing temperature is increased from 600 to 1000 °C. This indicates that the electrocatalytical behavior of NG for ORR is significantly influenced by the annealing temperature. The exact kinetic parameters including electron transfer number (n) and kinetic current density (J_K) of the resulting NG were analyzed on the basis of Equation (1)[34] and the Koutecky–Levich equations[27,37] (see Supporting Information Figure S6), respectively.

$$n = 4I_D/(I_D + I_R/N) \quad (1)$$

where $N = 0.36$ is the current collection efficiency, I_D is the disk current, and I_R is the ring current. Obviously, the NG prepared at 600 °C exhibits two coexisting pathways involving both the two-electron and four-electron transfers, with a very low kinetic current density of 2.5 mA cm^{-2} (Figure 4c,d). Nevertheless, with the increase of the temperature from 600 to 1000 °C, the electron transfer number of NG approaches the derived modul of four for ORR. The kinetic current density of NG is also strongly governed by the heating temperature. Typically, the highest current density of 7.8 mA cm^{-2} is observed for NG-900. This value is even higher than that of commercial Pt-C (J_k = 5.1 mA cm^{-2}) at the same testing conditions (Figure 4c,d). Owing to the metal-free fabrication procedure, the different electrocatalytical activity of N-doped graphene for ORR can be attributed exclusively to the incorporation of various nitrogen portions in the graphene structure. Based on the XPS studies (Figure 3c), it is reasonable to believe that the increase of the electrocatalytic activity of NG prepared between 600 and 900 °C is ascribed to the enhancement of both pyridinic and graphitic N contents, while the lower activity of NG1000 with respect to NG900 should be due to the reduced pyridinic N in the matrix. Given that the two types of nitrogen atoms with strong electron-accepting ability can create a net positive charge on the adjacent carbon atoms in the resulting NG sheets, they assist the adsorption of oxygen and can readily attract electrons from the anode, thus facilitating the ORR.[37]

Meanwhile, the electrocatalytic activity of S-doped graphene was also investigated via RRDE linear sweep voltammetry under the same testing conditions. As shown in **Figure 5**, all the S-doped graphenes show the obvious electrocatalytic activity for oxygen reduction reactions. And the electrocatalytic activity of SG is strongly dependant on the annealing temperature, similar to that of N-doped graphene. As the annealing temperature increasing from 500 to 900 °C, the electron transfer number of SG slightly decreases from 3.5 to 3.2 (Figure 5b). Associated with our XPS analysis of SG samples, it is reasonable to believe that the decrease of the electron transfer number of SG should be ascribed to the reduction of the amount of sulfur (from 1.7% to 1.2%) in SG samples since the S-C bonds should play a key role to affect the catalytic process of SG for ORR, similar to that of N-C bonds in NG. In addition, we find that the kinetic current density of SG900 (5.3 mA cm^{-2}) is significantly lower than that of NG900 (7.8 mA cm^{-2}). The reason for this should be that the S-C bonds are predominately at the edges and the defect sites of SG (demonstrated by our XPS analysis), which results in the lower content and inhomogeneous distribution of sulfur in SG compared to that of nitrogen in NG. Therefore, to improve the content and distribution of sulfur on graphene should be a promising way to improve the electrocatalytic activity of S-doped graphene for ORR.

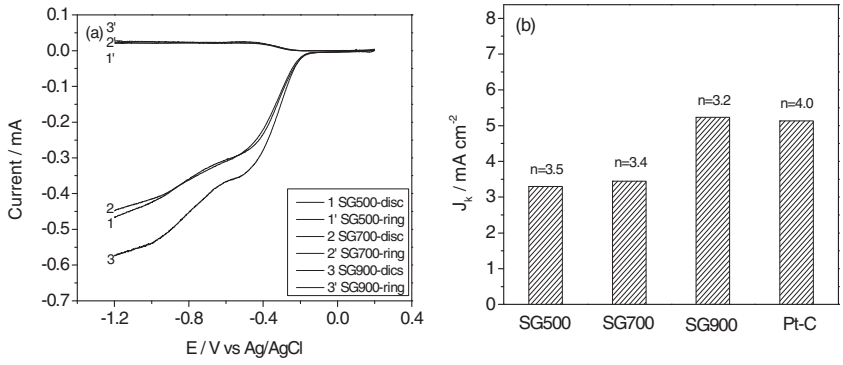

Figure 5. Electrocatalytic activity of S-doped graphene for ORR. a) Rotating ring disk electrode (RRDE) linear sweep voltammograms of SG500, SG700, and SG900 at a rotation rate of 1600 rpm. b) Electrochemical activity given as the kinetic-limiting current density (J_k) and electron transfer number (n) of SG500, SG700, SG900, and Pt-C at –0.50 V.

N and S-doped graphene as well as commercial Pt-C were further compared by separately introducing O_2 and fuel molecules (e.g., methanol) into the electrolyte to examine their possible selectivity and crossover effects via chronoamperometric measurements. As displayed in **Figure 6**, in the cases of NG and SG, the strong and stable amperometric responses are observed after the introduction of O_2 into the electrolyte, which remain unchanged after the subsequent addition of methanol. In contrast, a distinct change for Pt/C is detected once methanol is added under the same testing conditions. This result suggests that both N and S-doped graphenes indeed exhibits a high selectivity for ORR with a remarkable tolerance to crossover effects. More importantly, the durabilities of N and S-doped graphenes are higher than that of Pt-C. As shown in Figure S7b (Supporting Information), after 30 000 seconds of reaction at –0.3 V, 65% and 73% of the current density of N and S-doped graphenes towards ORR can be maintained, respectively, which are higher than that of the Pt-C catalyst (55%).

3. Conclusions

In summary, we have described a simple and cost-effective approach for the production of heteroatom (N or S)-doped graphene via thermal reaction between graphene oxide and guest gases (NH_3 or H_2S) on the basis of sandwich-like, ultrathin graphene oxide-porous silica sheets at high temperatures. Our studies prove for the first time that sulphur can be doped into graphene sheets in a major form of thiophene-like S, whereas nitrogen can be incorporated into graphene with three types of binding configurations including pyridinic-N, pyrrolic-N and graphitic-N. Moreover, the resulting N and S-doped graphene sheets showed excellent electrocatalytic activity, long durability and high selectivity when they were employed as metal-free catalyst for ORR. We believe that our synthetic approach can be further extended to produce a series of heteroatom-doped graphenes such as B, F and P-graphene with broad applications in electronics, fuel cells, supercapacitors and lithium ion batteries.

4. Experimental Section

Graphene oxide was synthesized from natural graphite flakes by the Hummers method,[19] and the ultrathin graphene oxide-porous silica sheets were fabricated by a modified approach in paper.[9] In a typical experiment, graphene oxide (30 mg) was firstly suspended in an aqueous solution containing CTAB (1 g) and NaOH (40 mg), and then ultrasonically treated for 3 h. After magnetic stirring for 2 h at 40 °C, 0.25 mL of tetraethylorthosilicate (TEOS) was slowly added to the above mixture. After reaction for 12 h, the desired ultrathin graphene oxide-mesoporous silica sheets were obtained by washing with warm ethanol, separation and dryness. N and S-doped graphene were produced by thermal reaction between resulting graphene oxide-mesoporous silica sheets and NH_3 and H_2S gas, respectively, at different temperatures (500–1000 °C) and subsequent removal of silica by alkaline or HF solution.

The morphology and microstructure of the samples were investigated by TEM (Philips EM 420), HRTEM (Philips Tecnai F20), AFM (Veeco Dimension 3100), EDX (Philips Tecnai F20), and XPS (VG ESCA 2000) measurements. Nitrogen sorption isotherms and BET surface area were measured at 77 K with a Micromeritcs Tristar 3000 analyzer (USA). The Raman spectra of dried samples were obtained on Lab-RAM HR800 with excitation by an argon ion laser (514.5 nm). The procedure of glass carbon rotating disk electrode (5 mm in diameter, from Pine Research Instrumentation) pretreatment and modification were as follows: prior to use, the working electrode was polished mechanically with 0.5 μm diamond down to 0.05 μm alumina slurry to obtain a mirror-like surface and then washed with Mill-Q water and acetone and allowed to dry. 1 mg N-doped graphene was dissolved in 1 mL solvent mixture of Nafion (5%) and water (V: V ratio = 1:9) by sonication. For comparison, a commercially available catalyst of 30 wt% Pt supported on black carbon (fuel cell grade) was used and 1 mg/ml Pt-C suspension was also prepared as the same procedure described above. Subsequently, a 7.5 μg portion of catalyst (NG or Pt-C) was introduced onto the surface of glassy carbon electrodes using a microsyringe. And then the electrode was allowed to dry at RT for 12 h before measurement.

Electrochemical experiments were conducted using a computer-controlled potentionstation (CHI

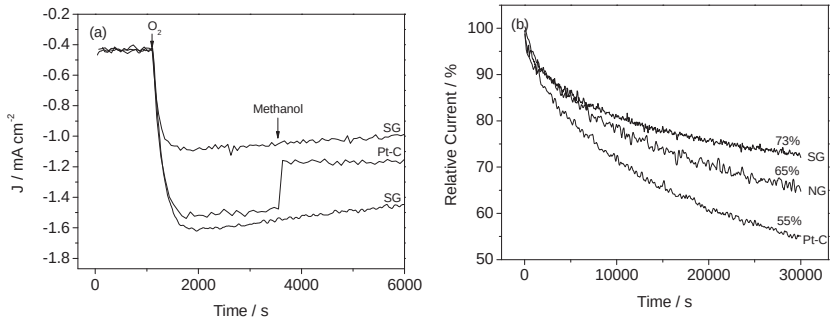

Figure 6. a) Current-time (*I-t*) chronoamperometric responses of NG, SG, and Pt/C electrodes at –0.3 V in 0.1 M KOH solution (1600 rpm) followed by separately introducing O_2 and methanol (0.3 M). b) *I-t* chronoamperometric responses of NG, SG, and Pt/C electrode at –0.3 V in O_2-saturated 0.1 M KOH solution at a rotation rate of 1600 rpm.

760D, CH Instrument, USA). A conventional three-electrode cell was employed incorporating a working glass carbon RRDE (Pine Research Instrumentation), an Ag/AgCl, KCl (3 M) electrode as reference electrode, and a Pt electrode as counter electrode. All potentials were measured and reported vs. the Ag/AgCl, KCl (3 M) reference electrode. The experiments were carried out in O_2 saturated 0.1 M KOH solution for the oxygen reduction reaction. The potential range was cyclically scanned between -1.2 and +0.2 V at different scan rate of 100 mV/s at the ambient temperature after purging O_2 or Ar gas for 15 min. RRDE measurements were conducted at different rotation rates from 225 to 2500 rpm.

Supporting Information

Supporting Information is available from the Wiley Online Library or from the author.

Acknowledgements

This work was financially supported by the Max Planck Society through the program ENERCHEM, DFG Priority Program SPP 1355, DFG MU 334/32-1, DFG Priority Program SPP 1459, BMBF LiBZ Project, ESF Project GOSPEL (Ref Nr: 09-EuroGRAPHENE-FP-001), EU Project GENIUS and ERC grant on NANOGRAPH.

Received: January 19, 2012
Published online: May 18, 2012

[1] K. S. Novoselov, Z. Jiang, Y. Zhang, S. V. Morozov, H. L. Stormer, U. Zeitler, J. C. Maan, G. S. Boebinger, P. Kim, A. K. Geim, *Science* **2007**, *315*, 1379.
[2] K. P. Loh, Q. L. Bao, P. K. Ang, J. X. Yang, *J. Mater. Chem.* **2010**, *20*, 2277.
[3] C. Lee, X. D. Wei, J. W. Kysar, J. Hone, *Science* **2008**, *321*, 385.
[4] X. L. Li, X. R. Wang, L. Zhang, S. W. Lee, H. J. Dai, *Science* **2008**, *319*, 1229.
[5] P. K. Ang, W. Chen, A. T. S. Wee, K. P. Loh, *J. Am. Chem. Soc.* **2008**, *130*, 14392.
[6] M. D. Stoller, S. J. Park, Y. W. Zhu, J. H. An, R. S. Ruoff, *Nano Lett.* **2008**, *8*, 3498.
[7] S. M. Paek, E. Yoo, I. Honma, *Nano Lett.* **2009**, *9*, 72.
[8] S. B. Yang, X. L. Feng, S. Ivanovici, K. Müllen, *Angew. Chem. Int. Ed.* **2010**, *49*, 8408.
[9] S. B. Yang, X. L. Feng, L. Wang, K. Tang, J. Maier, K. Müllen, *Angew. Chem. Int. Ed.* **2010**, *49*, 4795.
[10] S. B. Yang, G. L. Cui, S. P. Pang, Q. Cao, U. Kolb, X. L. Feng, J. Maier, K. Müllen, *ChemSusChem* **2010**, *3*, 236.
[11] P. A. Denis, R. Faccio, A. W. Mombru, *ChemPhysChem* **2009**, *10*, 715.
[12] B. Uchoa, A. H. C. Neto, *Phys. Rev. Lett.* **2007**, *98*.
[13] S. F. Huang, K. Terakura, T. Ozaki, T. Ikeda, M. Boero, M. Oshima, J. Ozaki, S. Miyata, *Phys. Rev. B* **2009**, *80*.
[14] S. Y. Wang, D. S. Yu, L. M. Dai, D. W. Chang, J. B. Baek, *ACS Nano* **2011**, *5*, 6202.
[15] L. T. Qu, Y. Liu, J. B. Baek, L. M. Dai, *ACS Nano* **2010**, *4*, 1321.
[16] D. C. Wei, Y. Q. Liu, Y. Wang, H. L. Zhang, L. P. Huang, G. Yu, *Nano Lett.* **2009**, *9*, 1752.
[17] N. Li, Z. Y. Wang, K. K. Zhao, Z. J. Shi, Z. N. Gu, S. K. Xu, *Carbon* **2010**, *48*, 255.
[18] X. L. Li, H. L. Wang, J. T. Robinson, H. Sanchez, G. Diankov, H. J. Dai, *J. Am. Chem. Soc.* **2009**, *131*, 15939.
[19] W. S. Hummers, R. E. Offeman, *J. Am. Chem. Soc.* **1958**, *80*, 1339.
[20] Y. C. Si, E. T. Samulski, *Chem. Mater.* **2008**, *20*, 6792.
[21] D. Li, M. B. Muller, S. Gilje, R. B. Kaner, G. G. Wallace, *Nat. Nanotechnol* **2008**, *3*, 101.
[22] P. M. Ajayan, W. Gao, L. B. Alemany, L. J. Ci, *Nat. Chem* **2009**, *1*, 403.
[23] R. S. Ruoff, M. D. Stoller, S. J. Park, Y. W. Zhu, J. H. An, *Nano Lett.* **2008**, *8*, 3498.
[24] S. Stankovich, D. A. Dikin, R. D. Piner, K. A. Kohlhaas, A. Kleinhammes, Y. Jia, Y. Wu, S. T. Nguyen, R. S. Ruoff, *Carbon* **2007**, *45*, 1558.
[25] K. R. Lee, K. U. Lee, J. W. Lee, B. T. Ahn, S. I. Woo, *Electrochem. Commun.* **2010**, *12*, 1052.
[26] S. B. Yang, X. L. Feng, L. J. Zhi, Q. A. Cao, J. Maier, K. Müllen, *Adv. Mater.* **2010**, *22*, 838.
[27] R. L. Liu, D. Q. Wu, X. L. Feng, K. Müllen, *Angew Chem. Int. Ed.* **2010**, *49*, 2565.
[28] Y. Wang, Y. Y. Shao, D. W. Matson, J. H. Li, Y. H. Lin, *ACS Nano* **2010**, *4*, 1790.
[29] X. Q. Wang, J. S. Lee, Q. Zhu, J. Liu, Y. Wang, S. Dai, *Chem. Mater.* **2010**, *22*, 2178.
[30] F. Buckel, F. Effenberger, C. Yan, A. Golzhauser, M. Grunze, *Adv. Mater.* **2000**, *12*, 901.
[31] I. Herrmann, U. I. Kramm, J. Radnik, S. Fiechter, P. Bogdanoff, *J. Electrochem. Soc.* **2009**, *156*, B1283.
[32] J. Y. Kim, P. J. Reucroft, M. Taghiei, V. R. Pradhan, I. Wender, *Energy Fuels* **1994**, *8*, 886.
[33] A. Turchanin, L. Kankate, A. Golzhauser, *Langmuir* **2009**, *25*, 10435.
[34] K. P. Gong, F. Du, Z. H. Xia, M. Durstock, L. M. Dai, *Science* **2009**, *323*, 760.
[35] W. Xiong, F. Du, Y. Liu, A. Perez, M. Supp, T. S. Ramakrishnan, L. M. Dai, L. Jiang, *J. Am. Chem. Soc.* **2010**, *132*, 15839.
[36] W. Yang, T. P. Fellinger, M. Antonietti, *J. Am. Chem. Soc.* **2012**, *134*, 4072.
[37] D. S. Yu, Q. A. Zhang, L. M. Dai, *J. Am. Chem. Soc.* **2010**, *132*, 15127.